# The potential of $^{223}$Ra and $^{18}$F-Fluoride imaging to predict bone lesion response to treatment with $^{223}$Ra-Dichloride in castration resistant prostate cancer

Iain Murray, Sarah J. Chittenden, Ana M. Denis-Bacelar, Cecilia Hindorf, Christopher C. Parker, Sue Chua, Glenn D. Flux

Iain Murray, Sarah J. Chittenden, Ana M. Denis-Bacelar, Cecilia Hindorf, Glenn D. Flux
Joint Department of Physics, Royal Marsden NHS Foundation Trust, Sutton, UK & the Institute of Cancer Research, London, UK

Sue Chua
Department of Nuclear Medicine, Royal Marsden NHS Foundation Trust, Sutton, UK

Christopher C. Parker
Department of Urology, Royal Marsden NHS Foundation Trust, Sutton, UK

Cecilia Hindorf
Department of Radiation Physics, Skåne University Hospital, Lund, Sweden (current affiliation)

**Corresponding Author:** Iain Murray, Physics Department, Royal Marsden NHS Hospital, Downs Rd. Sutton, Surrey, SM2 5PT, UK.

Email: iain.murray@icr.ac.uk

Tel: +44(0)2086613715

Fax: +44(0)2086433812

**Keywords:** Treatment Planning, Absorbed dose, $^{223}$Ra, Radium, alpha emitter, $^{18}$F, Fluoride.

**Acknowledgements**: NHS funding was provided to the NIHR Biomedical Research Centre at The Royal Marsden and the ICR. Data acquisition was funded by Bayer Healthcare Pharmaceuticals and Algeta ASA.

**Abstract**

The aims of this study were to calculate bone lesion absorbed doses resulting from a weight-based administration of $^{223}$Ra-dichloride, to assess the relationship between those doses and corresponding $^{18}$F-fluoride uptake and to assess the potential of quantitative $^{18}$F-fluoride imaging to predict response to treatment.

***Methods*** Five patients received two intravenous injections of $^{223}$Ra-dichloride, 6 weeks apart, at 110 kBq/kg whole-body weight. The biodistribution of $^{223}$Ra in metastatic lesions as a function of time after administration as well as associated lesion dosimetry were determined from serial $^{223}$Ra scans. PET/CT imaging using $^{18}$F-fluoride was performed prior to the first treatment (baseline), and at week 6 immediately before the second treatment and at week 12 after baseline.

***Results*** Absorbed doses to metastatic bone lesions ranged from 0.6 Gy to 44.1 Gy. For individual patients there was an average factor of 5.3 difference (range 2.5-11.0) between the maximum and minimum lesion dose. A relationship between lesion absorbed doses and serial changes in $^{18}$F-fluoride uptake was demonstrated ($r^2$ = 0.52). A log-linear relationship was demonstrated ($r^2$ = 0.77) between baseline measurements of $^{18}$F-fluoride uptake prior to $^{223}$Ra-dichloride therapy and changes in uptake 12 weeks after the first cycle of therapy. Correlations were also observed between both $^{223}$Ra and $^{18}$F-fluoride uptake in lesions (r = 0.75) as well as between $^{223}$Ra absorbed dose and $^{18}$F-fluoride uptake (r = 0.96).

***Conclusions*** There is both inter-patient and intra-patient heterogeneity of absorbed dose estimates to metastatic lesions. A relationship between $^{223}$Ra lesion absorbed dose and subsequent lesion response was observed. Analysis of this small group of patients suggests that baseline uptake of $^{18}$F-fluoride in bone metastases is significantly correlated with corresponding uptake of $^{223}$Ra, the associated $^{223}$Ra absorbed dose and subsequent lesion response to treatment.

## Introduction

Prostate cancer is the most commonly diagnosed non-cutaneous malignancy in men [1]. A significant number of patients will present with metastatic disease in the bones. Hormonal therapy is used as a first line treatment but in many cases the disease will eventually cease to respond to hormonal therapies.

In these circumstances, a range of palliative treatment options for bone metastases due to castration resistant prostate cancer (CRPC) are available, including a number of beta particle emitting radionuclides that are selectively taken up in areas of increased osteoblastic activity. Examples of such molecular radiotherapy treatments include $^{89}$Sr-chloride, $^{153}$Sm-EDTMP, $^{186}$Re-HEDP and $^{188}$Re-HEDP. Due to the range of the beta particles potential irradiation of normal bone marrow is anticipated and haematological toxicity is the main side-effect of such treatments [2].

Recently, treatment with $^{223}$Ra-dichloride has become available [3]. $^{223}$Ra is an alpha emitting radionuclide with a half-life of 11.4 days which also demonstrates increased uptake in regions of high osteoblastic activity. The short range of the alpha particles emitted (< 80 μm) enables high absorbed doses to be delivered to skeletal metastases whilst limiting the absorption of radiation within the bone marrow [4, 5].

The emissions from $^{223}$Ra include photons at energies that allow gamma camera imaging [6, 7]. However patients receiving $^{23}$Ra-dichloride are typically injected with 55 kBq/kg body mass resulting in limited count statistics in the images. As a result, tomographic imaging is impractical whilst 2D whole-body $^{223}$Ra images are characterised by significant levels of Poisson noise which can limit the positive identification of lesions for analysis. Nonetheless, two recent studies have used 2D gamma camera imaging to determine $^{223}$Ra absorbed doses according to the MIRD formalism, to measure biodistribution and to calculate normal organ dosimetry in patients treated with $^{223}$Ra-dichloride [8, 9]. In addition, Carrasquillo *et al* [10] used 2D gamma camera imaging to demonstrate early bone uptake of $^{223}$Ra as well as small bowel excretion. 2D gamma camera images were also used by Pacilio *et al* [11] to calculate the absorbed dose to bone metastases in patients receiving $^{223}$Ra-dichloride therapy. Notably, this group reported a range of lesion absorbed doses with an order of magnitude difference between the lowest and highest values. Earlier studies of $^{223}$Ra therapy have already demonstrated a relationship between the activity administered to a particular cohort of patients (e.g. 25 kBq/kg vs 50 kBq/kg) and the average change in pain index or PSA level across those cohorts [12, 13]. However to date there has been no

evidence of a relationship between the lesion absorbed dose and response to treatment with $^{223}$Ra-dichloride.

$^{18}$F-fluoride localises to the inorganic part of the bone, particularly in areas of osteoblastic activity, and has been used extensively for PET imaging of metastatic bone disease. Several studies have demonstrated superior sensitivity and specificity of $^{18}$F-fluoride imaging in comparison to conventional bone scintigraphy [14, 15]. Fluoride ions are incorporated into the hydroxyapatite crystal structure of the bone by substitution for hydroxyl (OH) ions. The relationship between osteoblastic and osteoclastic activity is believed to determine the amount of incorporation into the bone [16], given by.

$$Ca_{10}(PO_4)_6(OH)_2 + F_2^- \rightarrow Ca_{10}(PO_4)_6(F)_2 + 2OH^- \quad (1)$$

In common with $^{18}$F-fluoride, $^{223}$Ra localises to areas of osteoblastic activity and the hydroxyapatite crystal structure is also thought to be the target for $^{223}$Ra ions [4]. These ions are taken up into bone by ionic exchange with the calcium ions [17]. Given the common hydroxyapatite target, it can be hypothesised that pre-treatment $^{18}$F-fluoride PET imaging may provide theragnostic information regarding the response of lesions to treatment with $^{223}$Ra dichloride.

In this study the cumulated activity, the effective half-life and the range of absorbed doses delivered to a number of lesions were determined. The relationship between $^{223}$Ra absorbed doses and subsequent changes in $^{18}$F-fluoride uptake in these lesions was also investigated. To our knowledge such dose-response data for $^{223}$Ra-dichloride therapy has not previously been published. Furthermore, the potential for a single pre-treatment assessment of $^{18}$F-fluoride uptake to predict lesion response to $^{223}$Ra-dichloride treatment and to provide the basis for a surrogate dose-response relationship was investigated.

**Materials and Methods**

Data are presented from a *post-hoc* analysis of a phase I open-label clinical trial (NCT00667537) of $^{223}$Ra-dichloride in patients with bone metastases due to CRPC. Six patients with bone metastases from castration-resistant prostate cancer, as determined by $^{99m}$Tc-MDP bone scintigraphy no less than 6 weeks prior to treatment, were included in this study. Of the six patients recruited, five also underwent $^{18}$F-fluoride PET/CT imaging. Only these five patients were included in this post-hoc analysis.

Patients were scheduled to receive 100 kBq/kg of $^{223}$Ra-dichloride intravenously at baseline (therapy 1) and after 6 weeks (therapy 2). Following a revision of the primary standard for radionuclide calibrators [18, 19] it was retrospectively acknowledged that in fact patients received 110 kBq/kg. $^{18}$F-fluoride PET/CT imaging was performed at baseline up to 3 weeks before the first administration of $^{223}$Ra-dichloride, at 6 weeks just prior to the second administration of $^{223}$Ra-dichloride and at 12 weeks to assess treatment response. The mean age of patients that received both $^{223}$Ra-dichloride and $^{18}$F-fluoride was 63.2 years (range, 57 to 70 years). Normal $^{223}$Ra organ dosimetry in these patients has previously been reported [8]. A description of the changes in $^{18}$F-fluoride uptake, concluding that $^{18}$F-fluoride could be used as a biomarker to monitor response to $^{223}$Ra-dichloride has also been previously reported [20] as were eligibility criteria [8, 20]. Approval for the study was obtained from the appropriate research ethics committees and the national Administration of Radioactive Substances Advisory Committee, and all patients provided written informed consent.

### *$^{99m}$Tc-MDP Imaging*

Whole-body $^{99m}$Tc-MDP images were acquired 3 hours after injection of 600 MBq $^{99m}$Tc-MDP. Imaging was performed on a Forte gamma camera (Philips Medical Systems, Cleveland, OH, US) using a low energy high resolution collimator according to a protocol previously detailed. Whole-body views were acquired for approximately 20 minutes using a matrix size of 256 x 1024. Imaging was performed using an energy window set at 140 +/- 10% keV.

### *$^{223}$Ra Imaging*

Sets of whole-body $^{223}$Ra images were acquired in conjunction with each $^{223}$Ra-dichloride administration. Imaging was performed on a Forte gamma camera (Philips Medical Systems, Cleveland, OH, US) using a medium energy general purpose collimator according to a protocol previously detailed [6]. Whole-body and spot views were acquired for approximately 30 minutes each using matrix sizes of 256 x 1024 and 256 x 256 pixels respectively. Imaging was performed using an energy window set at 82 +/- 20% keV. The first scan was acquired within 0 – 4 h post-injection and subsequent scans were acquired at 24, 48, 96 and 144 h post-injection. All images were acquired post-void to reduce artefacts due to radioactivity in the bladder**.** The count rate for all measurements was sufficiently low (< 1 kcts/s over the

entire spectrum counted by the camera) that no correction was required for detector dead-time.

*$^{223}$Ra Image Analysis & Dosimetry*

Regions of interest (ROIs) around 29 metastatic bone lesions were initially delineated on the anterior and posterior $^{99m}$Tc-MDP whole-body images. Lesions corresponding to visible sites of increased $^{223}$Ra uptake were selected. For superscan patients (2/5), selected whole vertebrae were delineated as were the femoral heads. In one case an increased area of uptake in the right tibia was also selected. The $^{99m}$Tc images were manually registered to the $^{223}$Ra images using Hermes Hybrid Viewer (Hermes Medical, Sweden) to rigidly transform the images, thereby allowing transfer of the ROIs to the $^{223}$Ra whole-body and static images. The ROIs were then expanded in order to reduce the effect of spill-out due to partial volume effects and to limit the impact of any misregistration. Similarly to the work of Pacilio et al [11], a background correction for lesion uptake was determined from a region placed adjacent to the lesion ROI using the technique described by Buijs et al [21] whereby the background region was used to calculate an average background count per pixel. ROI delineation was performed by four observers comprising 3 experienced dosimetry physicists and 1 dual accredited consultant radiologist / nuclear medicine physician. The same consultant radiologist confirmed that all selected lesions were metastatic in nature.

Activity quantification was performed on the patient images according to either the conjugate view method or the single view effective point source method [22]. The conjugate view method was applied to those lesions situated close to a point equidistant between the anterior and posterior patient surface at the level of the lesion. The single view method was used to quantify uptake in lesions close to either the anterior or posterior surface which were not visible on the opposite view. Image counts were converted to activity using measured sensitivity and attenuation correction factors for $^{223}$Ra as previously detailed [6]. The depth of a lesion within a patient was measured on the CT scan associated with the baseline $^{18}$F-fluoride PET scan.

Metastatic bone lesion volumes were measured by applying a Fuzzy Locally Adaptive Bayesian (FLAB) segmentation algorithm, initially developed for accurate outlining of PET data for radiotherapy planning, to the corresponding lesion sites on the baseline $^{18}$F-fluoride PET images. [23].

The decay constant $\lambda$ associated with the effective half-life, $t_{1/2\ eff}$ and initial activity, $A_0$, of $^{223}$Ra in identified lesions was calculated by fitting a single exponential to the time activity

curve. The fit was constrained such that the effective half-life could not be greater than the physical half-life. Cumulated activity was calculated according to,

$$\tilde{A} = \frac{A_0}{\lambda} \qquad (2)$$

The total mean absorbed dose, D, to the target region included contributions from the decay of the daughter products of $^{223}$Ra ($^{219}$Rn, $^{215}$Po, $^{211}$Pb, $^{211}$Bi, $^{211}$Po, $^{207}$Tl) The absorbed doses delivered to metastatic lesions by each isotope were calculated using self-irradiation S-factors for unit density spheres [24], scaled for an assumed bone density of 1.3 g ml$^{-1}$ [25]. The absorbed dose is then given by

$$D = \sum_i \left[\tilde{A} \times S_i \times \left({}^{V_S}/_{V_t \times 1.3}\right)\right] \qquad (3)$$

where $S_i$ is the self-irradiation S-Factor for isotope *i* and spherical volume $V_s$; and $V_t$ is the lesion volume as determined by PET imaging. No radiation weighting factor was used to adjust the reported absorbed doses. It was assumed that the biodistribution of the daughter isotopes was the same as the $^{223}$Ra parent isotope [26].

*$^{18}$F-fluoride Imaging*

Repeated $^{18}$F-fluoride PET imaging was performed to assess treatment response. At each imaging time point, total body (vertex to feet) PET imaging was performed 1 h following injection of 250 MBq $^{18}$F-fluoride on a Gemini PET/CT scanner (Philips Medical Systems, Cleveland, OH, US). Data were acquired for 3.5 min per bed position following a low-current (50 mAs) CT scan performed for attenuation correction and lesion localisation.

*$^{18}$F-fluoride Image Analysis*

$^{18}$F-fluoride PET scans were assessed semi-quantitatively for evidence of response at the 6 and 12-week time points compared to the baseline pre-treatment scan. In the case of one patient, the third PET scan was rejected for analysis due to technical problems with the image acquisition. FLAB derived outlines of the 29 lesions identified on $^{99m}$Tc-MDP imaging were produced using an IDL routine incorporated into a Symbia.Net workflow (Siemens Healthcare, Germany). These were used to measure the $SUV_{mean}$ as well as the volume of each lesion. $SUV_{mean}$ values were corrected for partial volume effects as a function of lesion volume ($V_t$) using the following expression for recovery coefficient (RC) as described by Kessler et al [27] where $\sigma$ is the standard deviation of a Gaussian function describing the point spread function, determined by fitting equation 4 to the measured recovery curve

associated with an IEC NEMA image quality phantom filled with $^{18}$F. For the PET imaging described in this study a value of $\sigma$ = 4.3 mm was used.

$$RC = erf\left(\frac{\left[{}^{3V}/_{4\pi}\right]^{1/3}}{\sqrt{2}\sigma}\right) - \sqrt{{}^{2}/_{\pi}}\left(\frac{\left[{}^{3V}/_{4\pi}\right]^{1/3}}{\sigma}\right)e^{-\left(\frac{\left[{}^{3V}/_{4\pi}\right]^{2/3}}{2\sigma^2}\right)} \qquad (4)$$

The patient body mass and lesion volumes were used to convert values of $SUV_{mean}$ to percentage injected activity (%IA).

$$\%IA = \frac{SUV \times lesion\ volume[ml]}{(patient\ body\ mass[kg] \times 1000)} \quad (5)$$

Percentage changes in $SUV_{mean}$ relative to the baseline PET study were used to define the response to $^{223}$Ra-dichloride therapy on a lesion by lesion basis. Changes were measured at both 6 weeks and 12 weeks after baseline. Response to treatment after 6 weeks was plotted as a function of the $^{223}$Ra absorbed dose due to the first therapy. Response to treatment after 12 weeks was plotted as a function of the total $^{223}$Ra absorbed dose.

*$^{18}$F-fluoride and $^{223}$Ra Comparison*

To test the hypothesis that $^{18}$F-fluoride uptake is predictive of both, $^{223}$Ra uptake and subsequent lesion response, the %IA of $^{18}$F in each lesion at baseline was compared to %IA of $^{223}$Ra at the time of the first therapy administration. Additionally, the %IA of $^{18}$F in each lesion at 6 weeks post therapy 1 was compared to %IA of $^{223}$Ra at the time of the second therapy administration.

The $SUV_{mean}$ at baseline was compared to the calculated absorbed dose due to $^{223}$Ra uptake in lesions. In addition, response to treatment at 6 weeks and 12 weeks post $^{223}$Ra-dichloride was plotted as a function of baseline $SUV_{mean.}$. Figure 1 shows an example of all imaging ($^{223}$Ra WB imaging, $^{99m}$Tc WB imaging and $^{18}$F-fluoride PET/CT.)

*Uncertainty Analysis*

Data were analysed using Graphpad Prism software. The $^{223}$Ra lesion time activity curves were fitted with a mono-exponential function to estimate values for $A_0$ and $\lambda$ as well as $u(A_0)$ and $u(\lambda)$, the uncertainty in those estimates, and $r(A_0, \lambda)$ the covariance of $A_0$ and $\lambda$.

The overall uncertainty in the cumulated activity was calculated according to equation 6 [28]. The fractional uncertainty in the cumulated activity was used as an estimate of the fractional uncertainty in the absorbed dose estimate.

$$u(\tilde{A}) = \left( \left(\frac{\delta \tilde{A}}{\delta A_0}\right)^2 u^2(A_0) + \left(\frac{\delta \tilde{A}}{\delta \lambda}\right)^2 u^2(\lambda) + 2\left(\frac{\delta \tilde{A}}{\delta A_0}\right)\left(\frac{\delta \tilde{A}}{\delta \lambda}\right) u(A_0, \lambda) \right)^{0.5} = \left( \left(\frac{1}{\lambda}\right)^2 u^2(A_0) + \left(\frac{-A_0}{\lambda^2}\right)^2 u^2(\lambda) + 2\left(\frac{1}{\lambda}\right)\left(\frac{-A_0}{\lambda^2}\right) r(A_0, \lambda) u(A_0) u(\lambda) \right)^{0.5} \quad (6)$$

The uncertainties associated with the $^{18}$F-Fluoride uptake measurements were derived from the results of Lin et al [29] who reported a coefficient of variation of 6.6% for lesion $SUV_{mean}$.

*Statistical Analysis*

The distribution of absorbed doses and the log-transform of this distribution were tested for normality using the D'Agostino-Pearson criteria. The Kruskal-Wallis test and its associated p-value were used to compare the dose distributions resulting from the measurements of different observers.

Spearman rank correlation coefficients and their associated p-values were calculated between the %IA of $^{18}$F-fluoride and $^{223}$Ra in the lesions as well as between the lesion $SUV_{mean}$ and the $^{223}$Ra absorbed dose. Non-linear regression was performed to fit a log-linear function to the absorbed dose-response data as well as to the relationship between baseline $^{18}$F-fluoride $SUV_{mean}$ and subsequent percentage changes in $SUV_{mean}$ following therapy. The fits were weighted by the uncertainty associated with the response measurements. Coefficients of determination were calculated for these fits.

## Results

*$^{223}$Ra Image Analysis & Dosimetry*

A total of 29 metastatic lesions were identified on co-registered $^{99m}$Tc-MDP and $^{223}$Ra WB images. The dosimetry results for these lesions are summarised in Table 1. Absorbed doses ranged from 0.6±0.3 Gy to 44.1±16.4 Gy with a median absorbed dose of 4.1 Gy (see Figure 2). There was no significant difference in the observed absorbed doses determined from the lesion outlines of each operator (p=0.58). The log-transform of each distribution was found to be normally distributed. The median uncertainty in the lesion dose calculations (±1.0 Gy) was more than an order of magnitude less than the range of the calculated values. Approximately 80% of the absorbed dose in each lesion was due to alpha and beta particles emitted from the daughter isotopes. A full breakdown of the relative contribution of each isotope is given in Table 2. The effective half-life of $^{223}$Ra in lesions ranged from 44 hours to

274 hours (the physical half-life) with a median effective half-life of 136 hours (See Figure 3)).

A significant high correlation was observed between lesion uptake ($A_0$) at the time of the first therapy and the time of the second therapy 6 weeks later ($r = 0.88$, $p < 0.0001$). The relationship between the effective half-life of $^{223}$Ra measured at the two different time points was also significantly correlated ($r = 0.77$, $p < 0.0001$) as was the relationship between the lesion absorbed doses ($r = 0.85$, $p < 0.0001$). These relationships are shown in Figure 4.

*$^{223}$Ra – $^{18}$F-fluoride dose response relationship*

The relationship between lesion absorbed dose and the observed response as defined by percentage change in the $^{18}$F-fluoride $SUV_{mean}$ relative to baseline are shown in Figure 5. After 6 weeks there is no evident relationship between lesion dose and response ($r^2 = 0.07$). However after 12 weeks there is an apparent log-linear relationship ($r^2 = 0.54$) between the total absorbed dose from both therapies and the changes in the $^{18}$F-fluoride uptake. Based on the analysis of test-retest $^{18}$F-fluoride PET/CT imaging, Kurdziel et al [30] suggested a minimum percentage change of 21% should be used to identify real change in the $SUV_{mean}$ between two sequential scans of $^{18}$F-fluoride acquired 60 minutes post injection. For a change of > 21% in $SUV_{mean}$ of a lesion, a threshold of 5.0 Gy correctly identifies 94% of all responding lesions whilst no non-responding lesions are incorrectly identified as responding.

*$^{18}$F-fluoride and $^{223}$Ra Comparison*

The relationship between %IA $^{223}$Ra and %IA $^{18}$F-fluoride is shown in Figure 6. A significant high correlation ($r=0.71$, $p<0.0001$) was observed. Furthermore, a high correlation is demonstrated between therapy 1 lesion absorbed dose and baseline $^{18}$F-fluoride $SUV_{mean}$ ($r = 0.77$, $p<0.0001$) as well as between therapy 2 lesion absorbed dose and $^{18}$F-fluoride $SUV_{mean}$ at 6 weeks ($p<0.0001$). (Figure 7.)

*$^{18}$F-fluoride Image Analysis*

Figure 8 shows a log-linear dose response relationship between baseline $SUV_{mean}$ prior to treatment and the lesion responses as defined by percentage changes in $SUV_{mean}$. In common with the $^{223}$Ra dose-response relationship, no significant relationship was observed 6 weeks after the first treatment. However at 12 weeks after the first treatment, a well-defined log linear relationship was observed ($r^2 = 0.77$). If response is again defined as a change of >21% in the $SUV_{mean}$ of a lesion then a threshold between 17-20 partial volume

corrected $SUV_{mean}$ correctly identifies 100% of all responding lesions whilst no non-responding lesions are incorrectly identified as responding.

## Discussion

Absorbed doses in metastatic bone lesions ranged from 0.6 Gy to 44.1 Gy in this study. I.e. there is significant heterogeneity of absorbed dose across the patient population. For individual patients there was an average factor of 5.3 difference (range 2.5-11.0) between the maximum and minimum lesion dose. Emissions from the daughter isotopes of $^{223}$Ra contributed between 79% – 84% of this absorbed dose. The absorbed doses from $^{223}$Ra emissions only were 0.1 – 9.4 Gy which encompass the range observed in the study by Pacilio et al [11]. For deterministic cell killing effects using alpha emitters, a factor of 5 for relative biological effectiveness (RBE) has been suggested [31, 32]. However, this has not been validated in human studies and therefore no corrections for RBE were made to the dosimetry data presented in this study.

The limited count statistics associated with $^{223}$Ra whole-body imaging lead to uncertainties in the fitting of the time activity curves which in turn leads to the propagation of further uncertainty in the estimation of the absorbed dose. In this study the uncertainty associated with the absorbed dose estimates ranged from 0.03 Gy to 16.4 Gy. Nevertheless the median uncertainty in the lesion dose calculations (±1.0 Gy) was an order of magnitude less than the range of the calculated values and interobserver variation was not significant. No correlation was observed between uncertainty and lesion volume, nor between lesion absorbed dose and lesion volume. One way of reducing the uncertainty associated with these absorbed dose estimates could be to change the time points at which $^{223}$Ra images are acquired. In our study, the latest imaging time points were at 6 days after administration. Pacilio *et al* [11] imaged patients up to 24 days after administration, approximately 4 times the median effective half-life observed in our cohort and more in alignment with the MIRD recommendations for appropriate temporal sampling [22].

A further source of uncertainty associated with molecular radiotherapy dosimetry is the estimation of lesion volume. In this study, the FLAB segmentation technique was used to measure volume. This technique developed for radiotherapy outlining has been shown to be both accurate and reproducible [33]. The use of this particular algorithm reduces inter-operator variability in measurements of lesion volume to approximately 1% compared to

~15% for manual delineation [34]. In the example image shown in Figure 1, the PET derived outline of a rib lesion is seen to closely match the bony anatomy of the lesion demonstrated by the CT imaging. However, the use of a macroscopic volume is likely to give rise to a systematic error in the dose estimation since the true target volume, the endosteal layer, is an unknown fraction of the outlined volume.

Despite these uncertainties, a relationship between the absorbed dose to a lesion delivered over two cycles of therapy and the subsequent response as measured by $^{18}$F-fluoride imaging was demonstrated. The lack of an early response to $^{223}$Ra treatment has previously been observed and it was suggested that the flare phenomenon, whereby an increase in $^{18}$F-fluoride uptake is observed following treatment, may be partly responsible for this [35].

The hypothesised relationship between $^{18}$F-fluoride and $^{223}$Ra uptake was demonstrated (see Figure 6). The relationship is similar to the linear relationship between $^{223}$Ra and $^{99m}$Tc-MDP uptake previously demonstrated by Pacilio *et al* [11]. A strong correlation between $^{18}$F-fluoride uptake and $^{223}$Ra absorbed dose was also observed, despite a wide range in the $^{223}$Ra lesion effective half-life.

The association between the $^{18}$F-fluoride uptake and $^{223}$Ra absorbed dose may therefore explain the apparent dose-response relationship between the $SUV_{mean}$ of a lesion measured prior to treatment with $^{223}$Ra-dichloride and the subsequent changes in $SUV_{mean}$ following two administrations of $^{223}$Ra-dichloride (Figure 8).

The potential for $^{18}$F-fluoride to act as a surrogate measure of $^{223}$Ra absorbed dose is appealing for a number of reasons. First, there is a higher coefficient of determination ($r^2$ value) between the $^{18}$F-fluoride $SUV_{mean}$ and the lesion response ($r^2$ = 0.77, Figure 8B) compared to that between the lesion absorbed dose and the lesion response ($r^2$ = 0.52, Figure 5B). I.e. the $^{18}$F-fluoride uptake at baseline is a better indicator of the subsequent response than the absorbed dose estimate. This may reflect the greater uncertainty associated with the calculation of $^{223}$Ra absorbed dose from low count planar data. Second, the measurement of mean SUV within a lesion is an analysis technique more commonly used in routine clinical practice than the analysis of serial whole body images to calculate absorbed doses, although such dosimetry methodology is well established. Finally, the advantage of a surrogate measure for absorbed dose derived from a pre-treatment $^{18}$F-fluoride PET scan is that it represents prospective theragnostic information that could enable personalised treatment planning.

Earlier studies of $^{223}$Ra therapy have already demonstrated a relationship between the activity administered to a particular cohort of patients (e.g. 25 kBq/kg vs 50 kBq/kg) and the average change in pain index or PSA level across those cohorts [12, 13]. The wide range in the absorbed dose across multiple metastatic sites, along with the ability to image that dose

distribution, either directly or through surrogate $^{18}$F-fluoride PET imaging, suggests that there is scope to further optimise the delivery of $^{223}$Ra-dichloride treatment at an individual level.

This study is limited by the number of patients recruited to the trial. In particular, the upper end of the dose-response curves could be better defined by additional data points. Nonetheless, if the relationship between initial $^{18}$F-fluoride and the subsequent response to therapy observed in this investigation can be replicated in a larger patient cohort, $^{18}$F-fluoride PET imaging can potentially provide a quantitative method for optimising the potential of $^{223}$Ra-dichloride treatment for individual patients.

Therefore future trials would need to address several issues. Whilst this study suggests that the individual lesion absorbed doses are predictive of subsequent changes observed with functional imaging, the relationship between absorbed dose and other clinically relevant endpoints including pain index, changes in ALP or PSA levels or prolonged survival should be investigated and quantified. This would further support the previous analysis of these patients by Cook et al [20] that described a qualitative association between changes in the average SUVmax of selected lesions and changes in ALP and PSA.

In this study a relationship between $^{18}$F-fluoride uptake, $^{223}$Ra absorbed dose and lesion response was demonstrated for two treatments of 110 kBq/kg. Further studies are required to investigate these results for alternative administration schedules including the current standard regimen of 6 x 55kBq/kg. The relationship between baseline uptake of $^{18}$F-fluoride and response to two treatments of 100 kBq/kg demonstrated that non-responding lesions could be identified prior to therapy. This leads to the hypothesis that a subset of patients who would benefit from increased activities of $^{223}$Ra-dichloride could be identified. Again, a suitably designed clinical trial would be required to test this hypothesis.

## Conclusion

$^{223}$Ra lesion dosimetry performed using planar WB and static images of $^{223}$Ra distribution show a wide range of absorbed doses across multiple sites of metastases. Evidence of a relationship between the $^{223}$Ra absorbed dose to a lesion and the subsequent response defined by serial $^{18}$F-Fluoride imaging was observed.

A relationship was also observed between the $^{18}$F-Fluoride uptake prior to $^{223}$Ra-dichloride treatment and the subsequent lesion response, indicating that $^{18}$F-fluoride $SUV_{mean}$ could potentially act as a predictor of lesion absorbed dose. This is likely due to the fact that

uptake of $^{18}$F-fluoride in bone metastases is significantly correlated with both the corresponding uptake of $^{223}$Ra and the associated $^{223}$Ra absorbed dose. Larger trials are required to confirm these initial findings as well as to explore potential methodologies for optimising treatment.

**Funding**: NHS funding was provided to the NIHR Biomedical Research Centre at The Royal Marsden and the ICR. Data acquisition was funded by Bayer Healthcare Pharmaceuticals and Algeta ASA.

**Disclosure**: Christopher C. Parker consults for Bayer Healthcare Pharmaceuticals and Algeta ASA.

**Ethical approval**: Informed consent was obtained from all individual participants in this study. All procedures performed in studies involving human participants were in accordance with the ethical standards of the institutional and/or national research committee and with the 1964 Helsinki declaration and its later amendments or comparable ethical standards.

Table 1: $^{223}$Ra Lesion Dosimetry

| Patient number | Lesion Site | Vol [ml] | Therapy | Absorbed Dose [Gy] ($^{223}$Ra and daughter isotopes) | Effective Half-life [hrs] |
|---|---|---|---|---|---|
| 1 | *T5 vertebra* | *5.9* | 1 | *10.2 ± 1.5* | *273.6 ± 0.0** |
| | | | 2 | *11.3 ± 2.3* | *237.5 ± 180.9* |
| | *Left femoral head* | *29.1* | 1 | *3.6 ± 0.7* | *273.6 ± 0.0** |
| | | | 2 | *4.7 ± 0.2* | *273.6 ± 0.0** |
| | *C4 vertebra* | *8.5* | 1 | *10.9 ± 1.6* | *273.6 ± 0.0** |
| | | | 2 | *11.2 ± 1.2* | *273.6 ± 0.0** |
| | *Right SI joint* | *6.6* | 1 | *6.2 ± 1.1* | *273.6 ± 0.0** |
| | | | 2 | *8.5 ± 0.4* | *181.7 ± 23.8* |
| | *S1 vertebra* | *7.7* | 1 | *3.8 ± 0.6* | *273.6 ± 0.0** |
| | | | 2 | *4.3 ± 0.9* | *273.6 ± 0.0** |
| | *L3 vertebral process* | *3.7* | 1 | *7.3 ± 3.3* | *157.0 ± 141.0* |
| | | | 2 | *10.0 ± 1.7* | *273.6 ± 0.0** |
| | *Left pelvis (ischeum)* | *5.5* | 1 | *3.4 ± 1.0* | *273.6 ± 0.0** |
| | | | 2 | *4.4 ± 1.4* | *273.6 ± 0.0** |
| 2 | *L5 vertebra* | *41.2* | 1 | *6.2 ± 0.3* | *159.9 ± 23.7* |
| | | | 2 | *4.2 ± 0.7* | *127.4 ± 47.3* |
| | *T12 vertebra* | *1.2* | 1 | *43.8 ± 11.2* | *143.0 ± 100.1* |
| | | | 2 | *44.1 ± 16.4* | *66.6 ± 50.6* |
| | *R pelvis* | *7.1* | 1 | *4.9 ± 0.8* | *83.8 ± 24.9* |
| | | | 2 | *17.5 ± 2.9* | *218.9 ± 198.1* |
| | *L3 vertebra* | *5.6* | 1 | *10.4 ± 0.9* | *108.5 ± 22.1* |
| | | | 2 | *5.5 ± 0.5* | *102.6 ± 19.2* |
| | *R Rib9* | *2.8* | 1 | *6.4 ± 1.2* | *92.7 ± 36.7* |
| | | | 2 | *4.0 ± 0.9* | *59.5 ± 24.5* |
| | *Sternum* | *18.7* | 1 | *6.0 ± 0.4* | *91.0 ± 12.2* |
| | | | 2 | *5.2 ± 0.2* | *91.4 ± 7.7* |
| 3 | *Right Skull* | *39.9* | 1 | *1.6 ± 0.3* | *135.7 ± 90.1* |
| | | | 2 | *1.1 ± 0.2* | *94.6 ± 30.6* |
| | *Left Skull* | *1.9* | 1 | *1.5 ± 1.0* | *84.4 ± 153.3* |
| | | | 2 | *1.5 ± 0.7* | *136.9 ± 162.4* |
| | *T11 vertebra* | *9.2* | 1 | *4.9 ± 0.6* | *76.3 ± 23.2* |
| | | | 2 | *5.8 ± 1.2* | *83.8 ± 35.0* |
| | *L3 vertebra* | *10.8* | 1 | *1.5 ± 0.7* | *141.2 ± 282.8* |
| | | | 2 | *5.3 ± 1.8* | *76.5 ± 47.8* |
| | *L4 vertebra* | *22.9* | 1 | *1.7 ± 0.8* | *61.1 ± 69.7* |
| | | | 2 | *2.6 ± 0.3* | *71.7 ± 17.1* |
| | *Right Rib 7* | *13.9* | 1 | *4.0 ± 1.3* | *92.0 ± 41.0* |
| | | | 2 | *2.7 ± 0.5* | *61.0 ± 20.2* |
| 4 | *L2 vertebra* | *39.4* | 1 | *0.6 ± 0.3* | *70.9 ± 51.7* |
| | | | 2 | *1.0 ± 0.2* | *44.4 ± 20.3* |
| | *L3 vertebra* | *56.4* | 1 | *1.0 ± 0.4* | *66.8 ± 37.8* |
| | | | 2 | *1.0 ± 0.2* | *45.0 ± 17.1* |
| | *T12 vertebra* | *32.0* | 1 | *1.5 ± 0.1* | *178.3 ± 27.7* |
| | | | 2 | *1.2 ± 0.2* | *94.1 ± 7.7* |
| | *L femoral head* | *68.9* | 1 | *1.4 ± 0.1* | *114.4 ± 25.6* |
| | | | 2 | *1.1 ± 0.1* | *78.3 ± 12.0* |
| | *R femoral head* | *67.5* | 1 | *1.1 ± 0.2* | *94.0 ± 31.9* |
| | | | 2 | *1.0 ± 0.2* | *98.3 ± 34.9* |
| 5 | *L1 vertebra* | *45.5* | 1 | *1.8 ± 0.3* | *112.0 ± 43.6* |

| | | | | | |
|---|---|---|---|---|---|
| | | | 2 | *2.5 ± 0.2* | *240.7 ± 81.9* |
| | *T11 vertebra* | *42.3* | 1 | *2.2 ± 0.3* | *145.5 ± 53.2* |
| | | | 2 | *3.0 ± 0.0* | *232.0 ± 8.8* |
| | *Right Femoral Head* | *59.0* | 1 | *8.1 ± 0.5* | *273.6 ± 0.0** |
| | | | 2 | *7.0 ± 0.5* | *273.6 ± 0.0** |
| | *Left Femoral Head* | *105.0* | 1 | *3.6 ± 0.3* | *261.5 ± 87.3* |
| | | | 2 | *3.4 ± 0.0* | *257.2 ± 11.8* |
| | *Right tibia* | *66.8* | 1 | *5.7 ± 0.9* | *168.2 ± 86.7* |
| | | | 2 | *8.3 ± 1.3* | *273.6 ± 0.0** |

**Table 1: List of lesions, their location and estimated absorbed doses. * no uncertainty estimate of effective half-life was possible where the monoexponential fit reached the constraint of $^{223}$Ra physical half-life .**

Table 2: Relative absorbed dose from Ra223 and daughter isotopes

| Isotope | Contribution to total lesion dose [%] |
|---|---|
| *Ra-223* | *21.3* |
| *Rn-219* | *24.6* |
| *Ra-215* | *26.9* |
| *Pb-211* | *1.6* |
| *Bi-211* | *23.9* |
| *Po-211* | *0.1* |
| *Tl-207* | *1.7* |

**Table 2: Relative contribution of each isotope to lesion absorbed dose.**

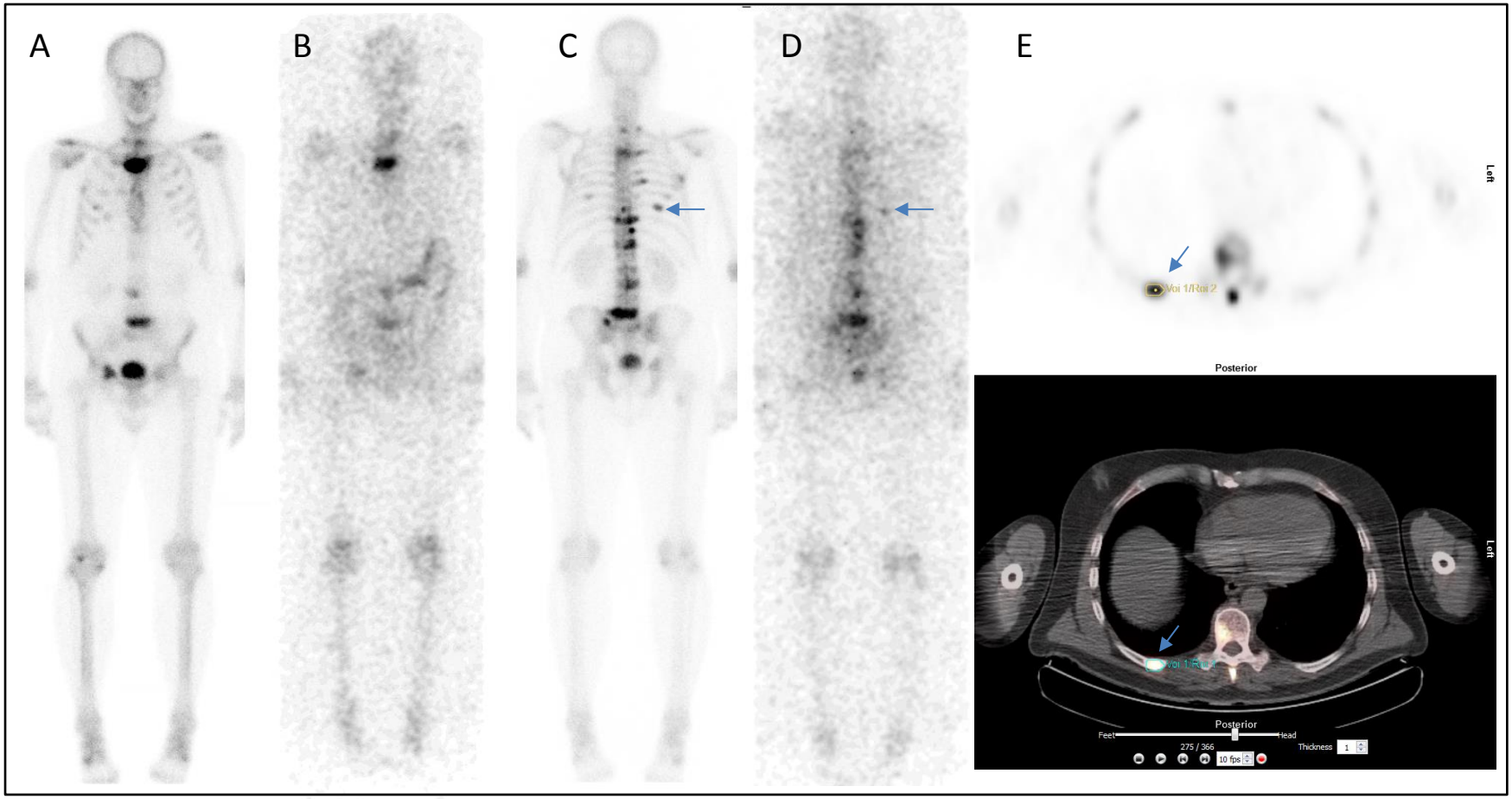


**Figure 1: Examples of acquired images for patient 2. A) and C) show $^{99m}$Tc-MDP whole-body imaging. B) and D) show $^{223}$Ra WB imaging 6 days after therapy administration. Arrows indicate uptake in posterior right rib. E) $^{18}$F-Fluoride PET/CT imaging at baseline including FLAB outlining of posterior right rib lesion used for volume estimation.**

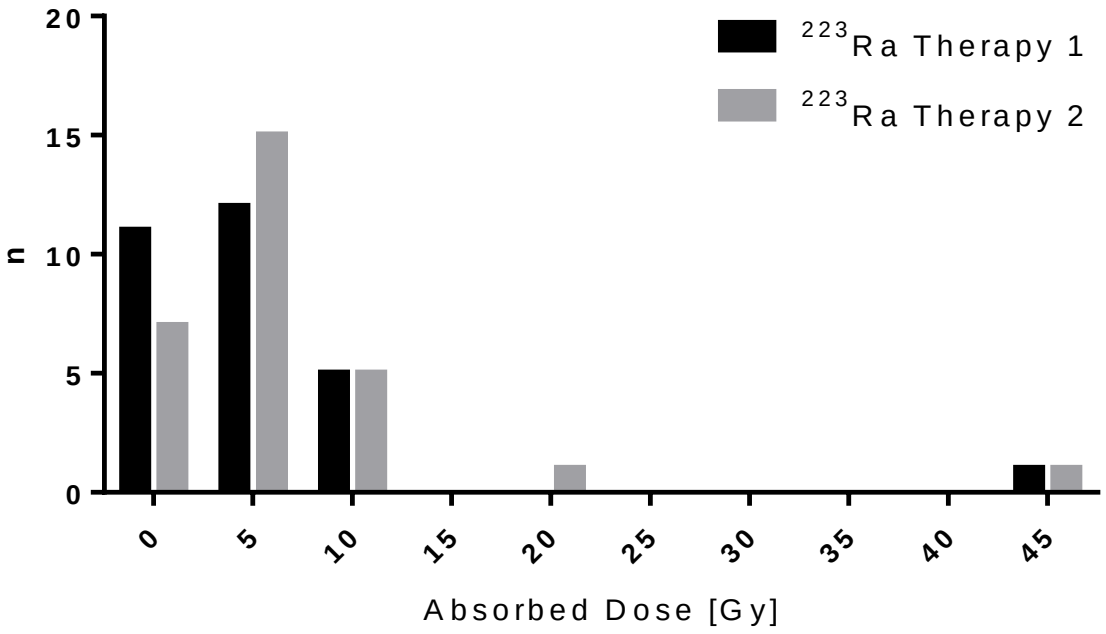


**Figure 2: Histogram of lesion absorbed dose. Data are shown for 29 lesions measured from 5 patients.**

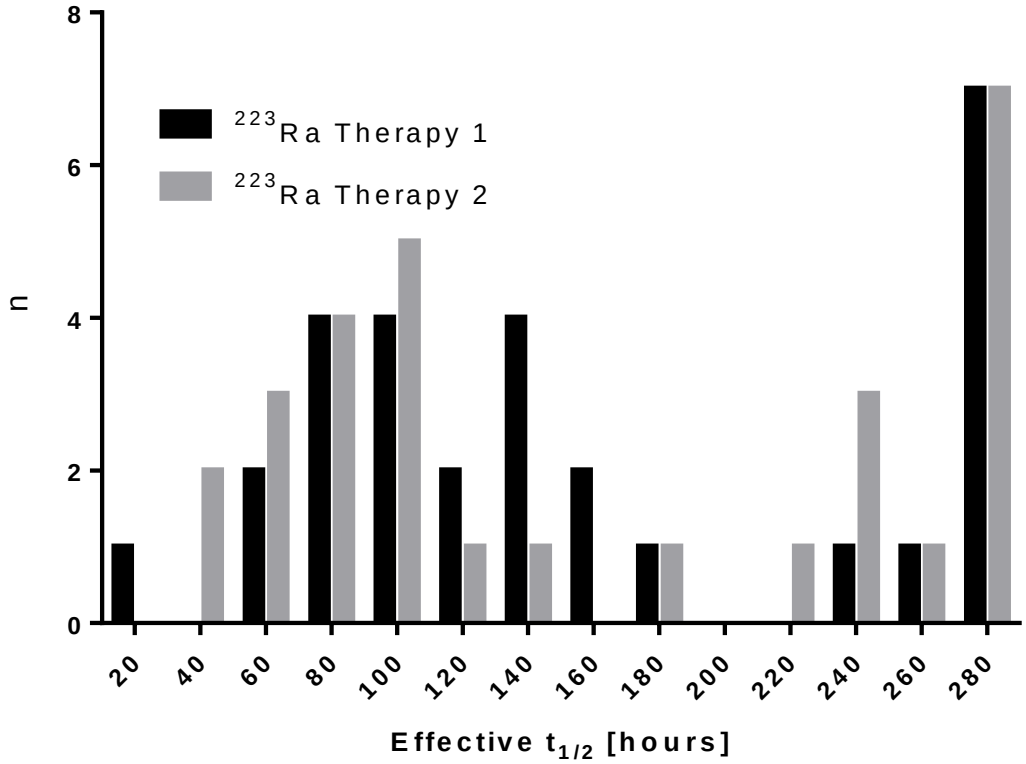


**Figure 3: Histogram of lesion effective half-life. Data are shown for 29 lesions measured from 5 patients.**

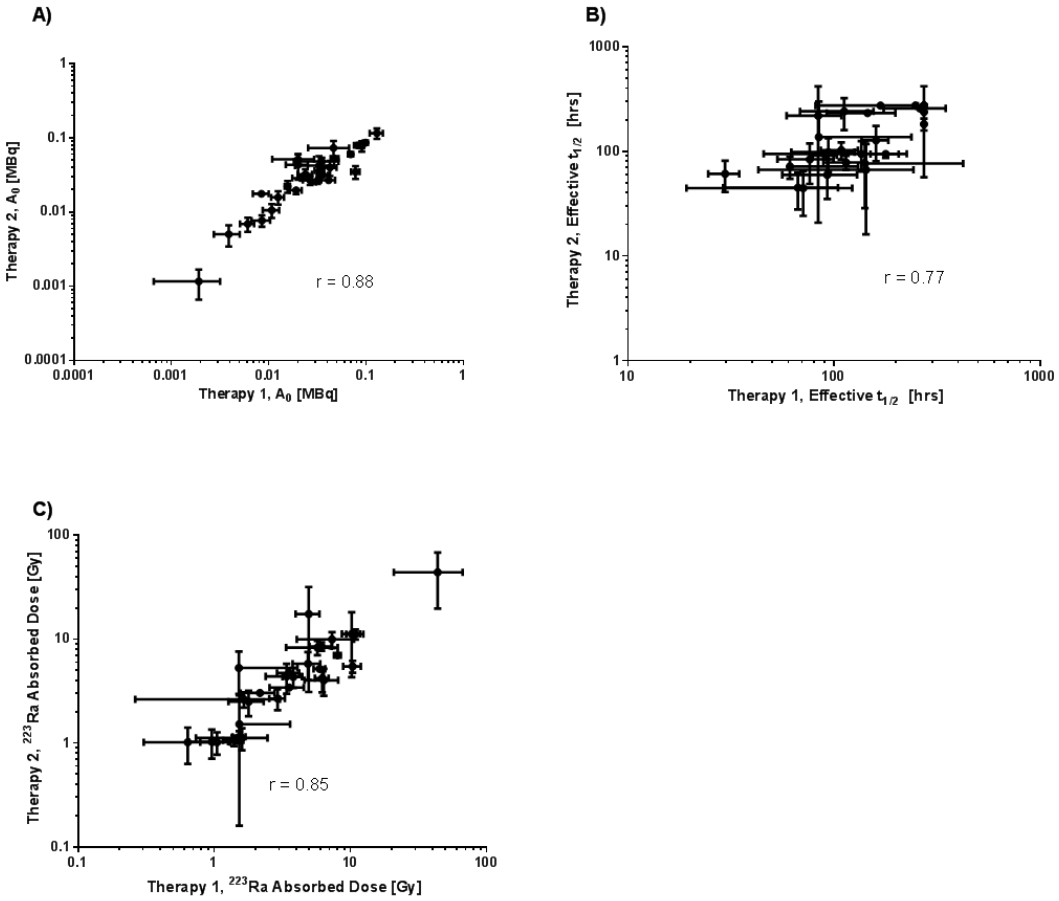


**Figure 4: Relationship between estimated absorbed dose parameters for therapy 1 and therapy 2. A) Initial lesion uptake of $^{223}$Ra, B) of $^{223}$Ra lesion effective half-life and C) lesion absorbed dose.**

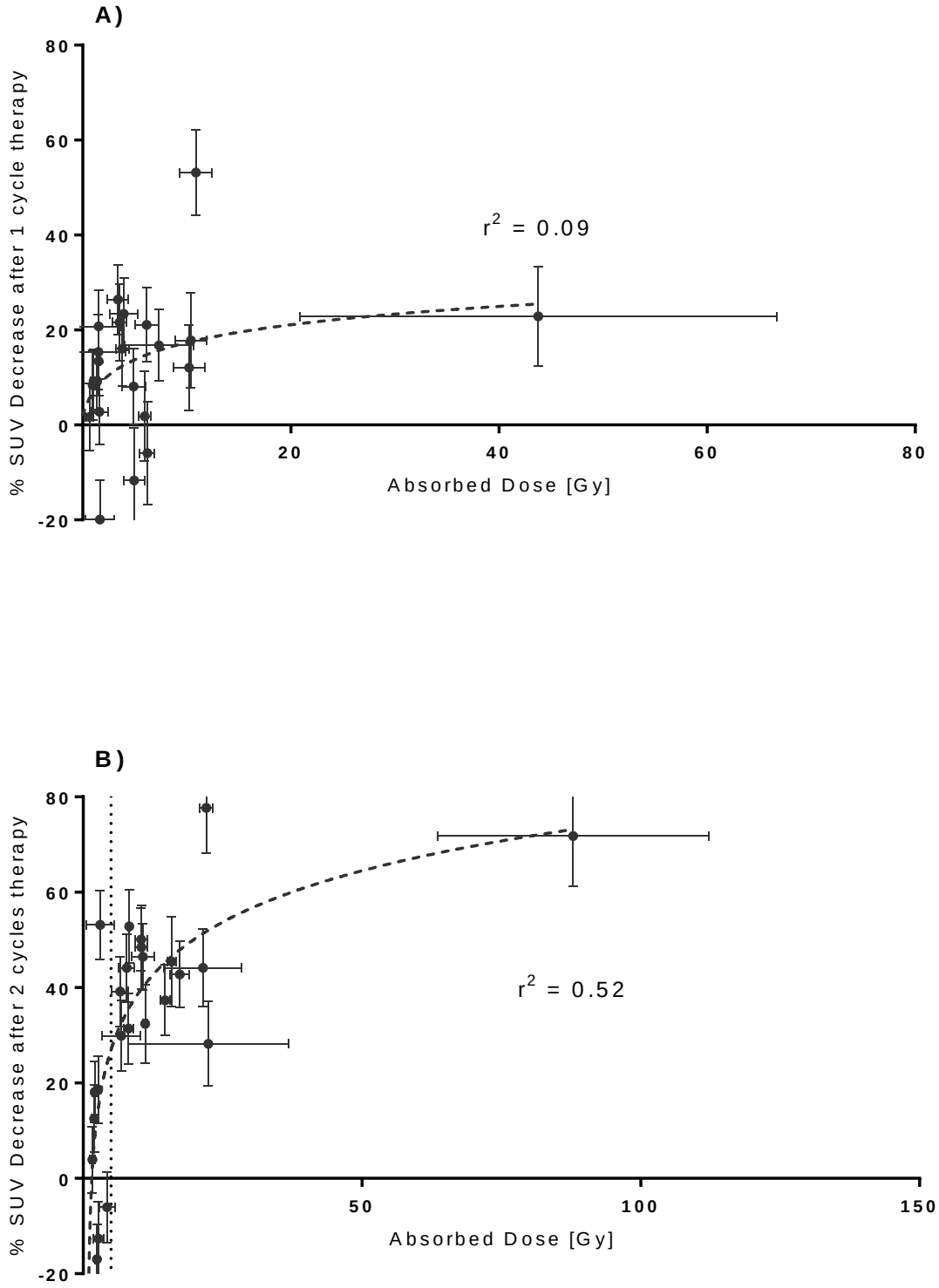


**Figure 5: Lesion response to $^{223}$Ra-dichloride treatment. (n=24 over 4 patients) A) Response to therapy 1 only assessed 6 weeks after baseline. B) Response to therapy 1 and 2 assessed 12 weeks after baseline.**

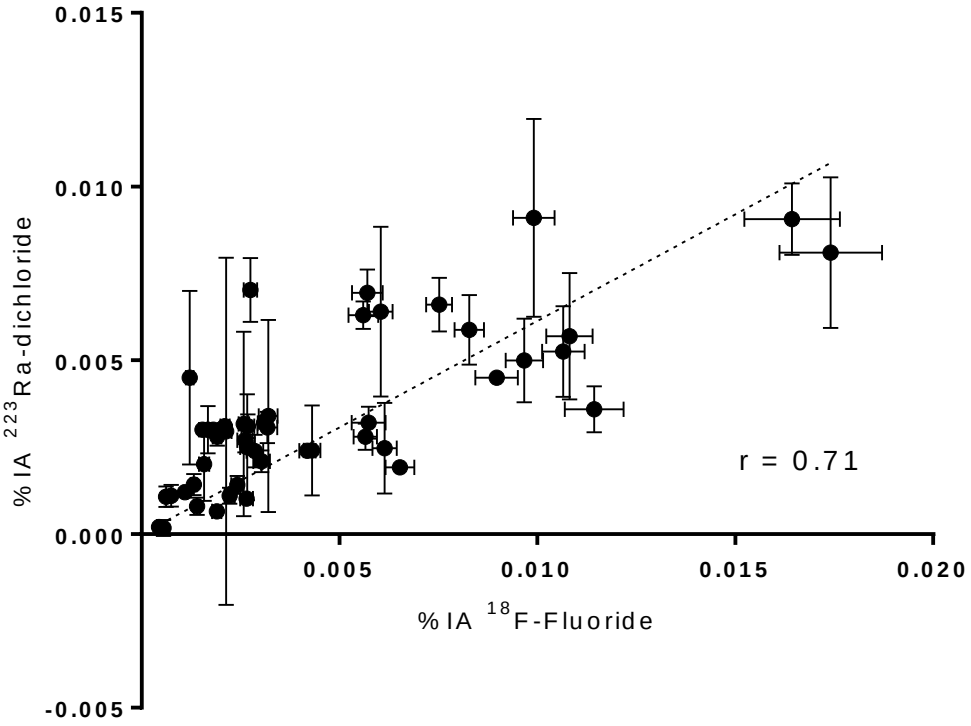


**Figure 6: Relationship between $^{223}$Ra uptake and $^{18}$F-Fluoride uptake. n = 58.**

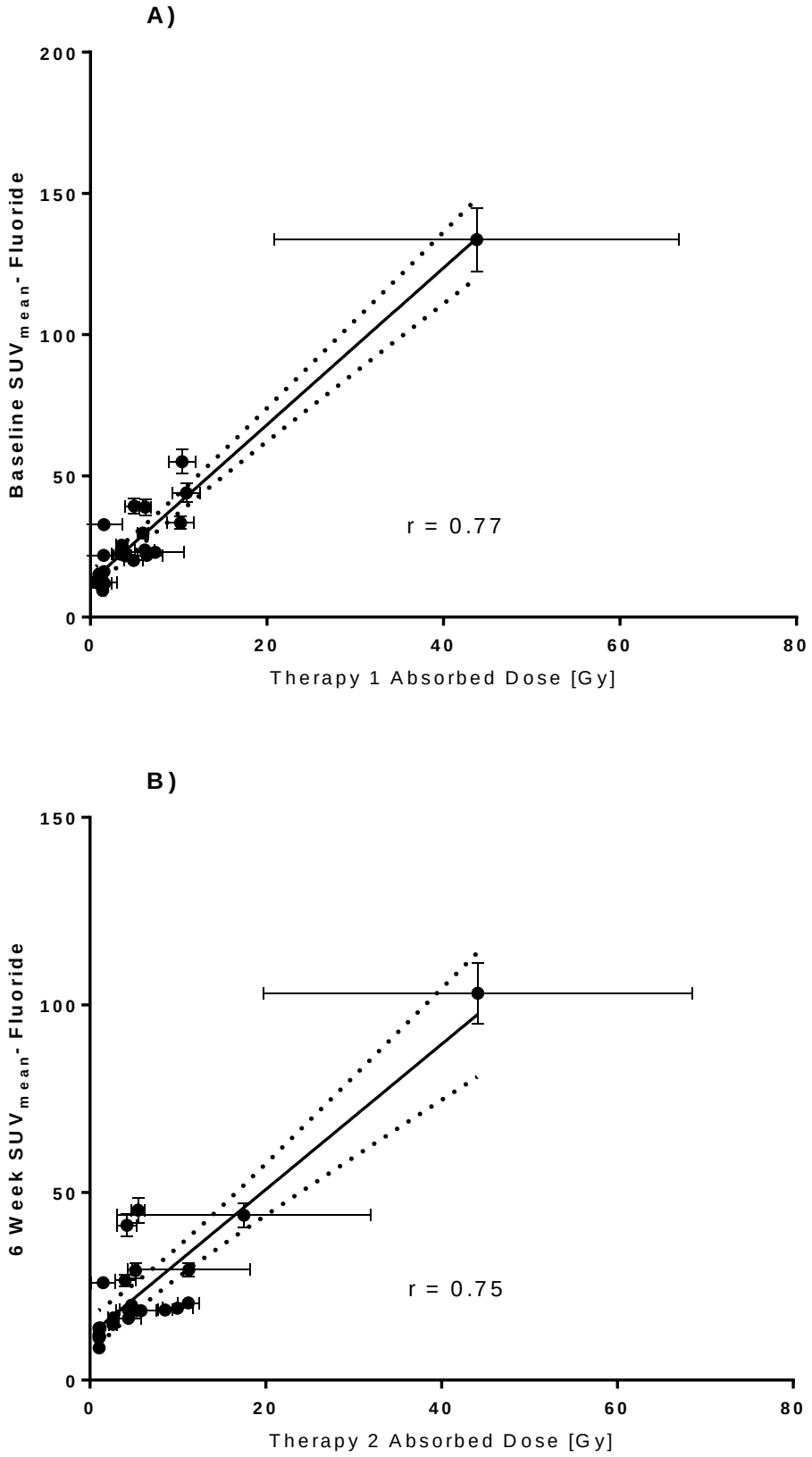


**Figure 7: Relationship between $^{223}$Ra absorbed dose to lesion and lesion $^{18}$F-fluoride $SUV_{mean}$ at the time of treatment. A) Dose from Therapy 1 vs Baseline PET. B) Absorbed dose from Therapy 2 vs 6 week PET.**

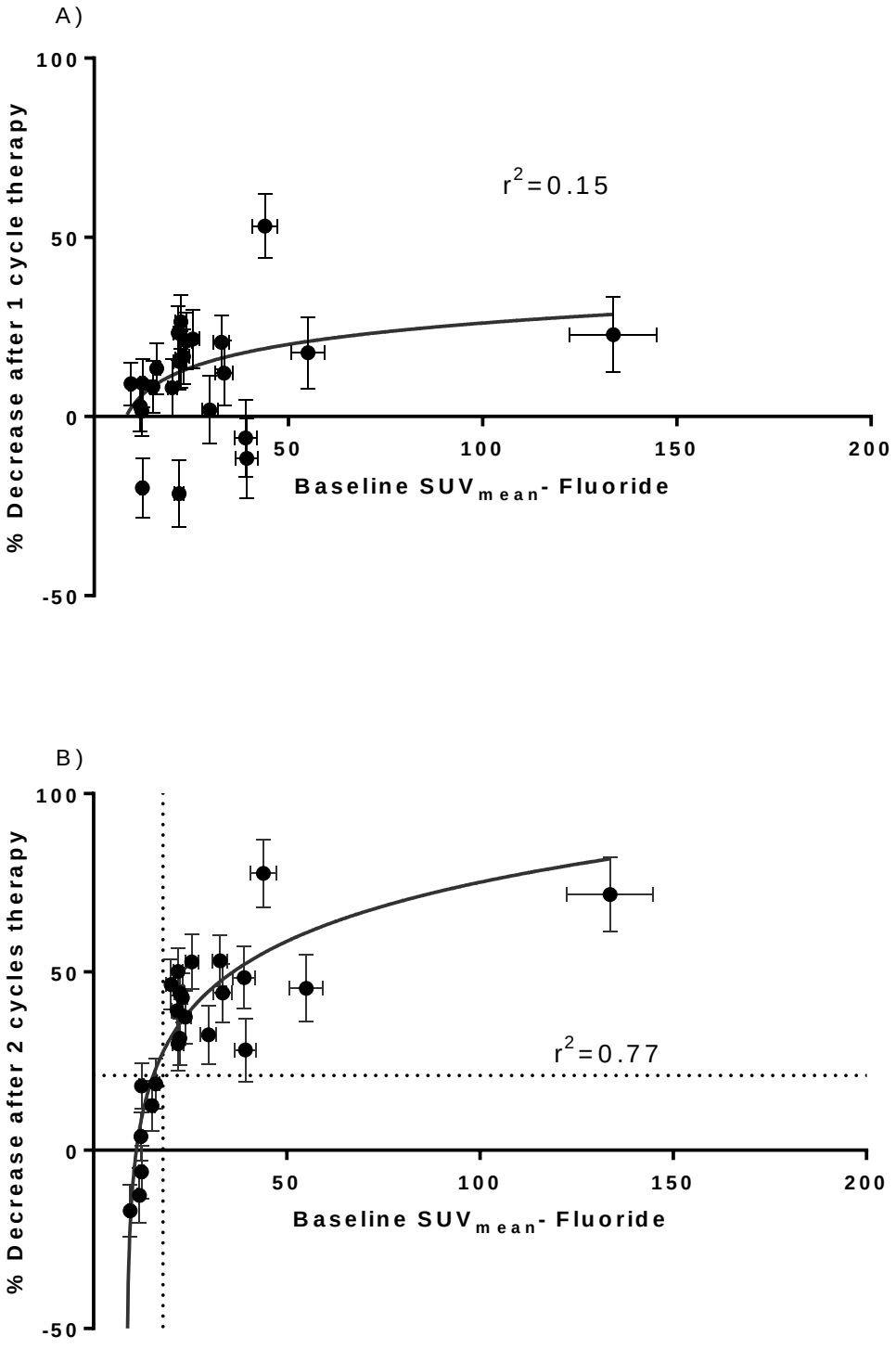


**Figure 8: Relationship between baseline $SUV_{mean}$ and subsequent response to $^{223}$Ra dichloride. A) Changes following one cycle of $^{223}$Ra-dichloride. B) Changes following two cycles of $^{223}$Ra-dichloride. (n=24 over 4 patients)**

References

1. Gartrell BA, Saad F. Managing bone metastases and reducing skeletal related events in prostate cancer. Nature reviews Clinical oncology. 2014;11:335-45. doi:10.1038/nrclinonc.2014.70.
2. Bodei L, Lam M, Chiesa C, Flux G, Brans B, Chiti A, et al. EANM procedure guideline for treatment of refractory metastatic bone pain. European journal of nuclear medicine and molecular imaging. 2008;35:1934-40. doi:DOI 10.1007/s00259-008-0841-y.
3. Florimonte L, Dellavedova L, Maffioli LS. Radium-223 dichloride in clinical practice: a review. European journal of nuclear medicine and molecular imaging. 2016;43:1896-909. doi:10.1007/s00259-016-3386-5.
4. Hobbs RF, Song H, Watchman CJ, Bolch WE, Aksnes AK, Ramdahl T, et al. A bone marrow toxicity model for Ra-223 alpha-emitter radiopharmaceutical therapy. Phys Med Biol. 2012;57:3207-22. doi:Doi 10.1088/0031-9155/57/10/3207.
5. Nilsson S, Larsen RH, Fossa SD, Balteskard L, Borch KW, Westlin JE, et al. First clinical experience with alpha-emitting radium-223 in the treatment of skeletal metastases. Clinical Cancer Research. 2005;11:4451-9. doi:10.1158/1078-0432.ccr-04-2244.
6. Hindorf C, Chittenden S, Aksnes AK, Parker C, Flux GD. Quantitative imaging of Ra-223-chloride (Alpharadin) for targeted alpha-emitting radionuclide therapy of bone metastases. Nuclear medicine communications. 2012;33:726-32.
7. Takahashi A, Miwa K, Sasaki M, Baba S. A Monte Carlo study on (223)Ra imaging for unsealed radionuclide therapy. Medical physics. 2016;43:2965. doi:10.1118/1.4948682.
8. Chittenden SJ, Hindorf C, Parker CC, Lewington VJ, Pratt BE, Johnson B, et al. A Phase 1, Open-Label Study of the Biodistribution, Pharmacokinetics, and Dosimetry of 223Ra-Dichloride in Patients with Hormone-Refractory Prostate Cancer and Skeletal Metastases. J Nucl Med. 2015;56:1304-9. doi:10.2967/jnumed.115.157123.
9. Yoshida K, Kaneta T, Takano S, Sugiura M, Kawano T, Hino A, et al. Pharmacokinetics of single dose radium-223 dichloride (BAY 88-8223) in Japanese patients with castration-resistant prostate cancer and bone metastases. Ann Nucl Med. 2016;30:453-60. doi:10.1007/s12149-016-1093-8.
10. Carrasquillo JA, O'Donoghue JA, Pandit-Taskar N, Humm JL, Rathkopf DE, Slovin SF, et al. Phase I pharmacokinetic and biodistribution study with escalating doses of (2)(2)(3)Ra-dichloride in men with castration-resistant metastatic prostate cancer. European journal of nuclear medicine and molecular imaging. 2013;40:1384-93. doi:10.1007/s00259-013-2427-6.
11. Pacilio M, Ventroni G, De Vincentis G, Cassano B, Pellegrini R, Di Castro E, et al. Dosimetry of bone metastases in targeted radionuclide therapy with alpha-emitting Ra-dichloride. European journal of nuclear medicine and molecular imaging. 2015. doi:10.1007/s00259-015-3150-2.
12. Nilsson S, Strang P, Aksnes AK, Franzen L, Olivier P, Pecking A, et al. A randomized, dose-response, multicenter phase II study of radium-223 chloride for

the palliation of painful bone metastases in patients with castration-resistant prostate cancer. European Journal of Cancer. 2012;48:678-86. doi:10.1016/j.ejca.2011.12.023.
13. Parker CC, Pascoe S, Chodacki A, O'Sullivan JM, Germa JR, O'Bryan-Tear CG, et al. A Randomized, Double-Blind, Dose-Finding, Multicenter, Phase 2 Study of Radium Chloride (Ra 223) in Patients with Bone Metastases and Castration-Resistant Prostate Cancer. Eur Urol. 2013;63:189-97. doi:10.1016/j.eururo.2012.09.008.
14. Segall GM. PET/CT with sodium 18F-fluoride for management of patients with prostate cancer. J Nucl Med. 2014;55:531-3. doi:10.2967/jnumed.113.133546.
15. Mick CG, James T, Hill JD, Williams P, Perry M. Molecular imaging in oncology: (18)F-sodium fluoride PET imaging of osseous metastatic disease. AJR American journal of roentgenology. 2014;203:263-71. doi:10.2214/AJR.13.12158.
16. Piert M, Zittel TT, Becker GA, Jahn M, Stahlschmidt A, Maier G, et al. Assessment of porcine bone metabolism by dynamic [F-18]fluoride ion PET: Correlation with bone histomorphometry. J Nucl Med. 2001;42:1091-100.
17. Neuman WF, Hursh JB, Boyd J, Hodge HC. ON THE MECHANISM OF SKELETAL FIXATION OF RADIUM. Annals of the New York Academy of Sciences. 1955;62:125-36. doi:10.1111/j.1749-6632.1955.tb35369.x.
18. Keightley J, Pearce A, Fenwick A, Collins S, Ferreira K, Johansson L. Standardisation of 223Ra by liquid scintillation counting techniques and comparison with secondary measurements. Applied radiation and isotopes : including data, instrumentation and methods for use in agriculture, industry and medicine. 2014;95C:114-21. doi:10.1016/j.apradiso.2014.10.009.
19. Zimmerman BE, Bergeron DE, Cessna JT, Fitzgerald R, Pibida L. Revision of the NIST Standard for (223)Ra: New Measurements and Review of 2008 Data. Journal of research of the National Institute of Standards and Technology. 2015;120:37-57. doi:10.6028/jres.120.004.
20. Cook GJR, Parker C, Chua S, Johnson B, Aksnes AK, Lewington VJ. F-18-fluoride PET: changes in uptake as a method to assess response in bone metastases from castrate-resistant prostate cancer patients treated with Ra-223-chloride (Alpharadin). EJNMMI research. 2011;1.
21. Buijs WCAM, Siegel JA, Boerman OC, Corstens FHM. Absolute organ activity estimated by five different methods of background correction. J Nucl Med. 1998;39:2167-72.
22. Siegel JA, Thomas SR, Stubbs JB, Stabin MG, Hays MT, Koral KF, et al. MIRD pamphlet no. 16: Techniques for quantitative radiopharmaceutical biodistribution data acquisition and analysis for use in human radiation dose estimates. J Nucl Med. 1999;40:37s-61s.
23. Hatt M, Cheze le Rest C, Turzo A, Roux C, Visvikis D. A fuzzy locally adaptive Bayesian segmentation approach for volume determination in PET. IEEE Trans Med Imaging. 2009;28:881-93.
24. Stabin MG, Siegel JA. Physical models and dose factors for use in internal dose assessment. Health Phys. 2003;85:294-310. doi:Doi 10.1097/00004032-200309000-00006.
25. Basic anatomical and physiological data: The skeleton. Annals of the ICRP. 1995;25:1-80. doi:http://dx.doi.org/10.1016/S0146-6453(00)80004-4.
26. Hindorf C. Dosimetry for radionuclide therapy with 223Ra-Cl2 with the biokinetics for the daughters measured separately. In preparation.

27. Kessler RM, Ellis JR, Eden M. ANALYSIS OF EMISSION TOMOGRAPHIC SCAN DATA - LIMITATIONS IMPOSED BY RESOLUTION AND BACKGROUND. Journal of Computer Assisted Tomography. 1984;8:514-22. doi:10.1097/00004728-198406000-00028.
28. BIPM, IEC, IFCC, ILAC, ISO, IUPAC, et al. Evaluation of measurement data - Guide to the expression of uncertainty in measurement. Joint Committee for Guides in Metrology (JCMG). 2008;101.
29. Lin C, Bradshaw TJ, Perk TG, Harmon S, Eickhoff J, Jallow N, et al. Repeatability of Quantitative 18F-NaF PET: A Multicenter Study. J Nucl Med. 2016. doi:10.2967/jnumed.116.177295.
30. Kurdziel KA, Shih JH, Apolo AB, Lindenberg L, Mena E, McKinney YY, et al. The kinetics and reproducibility of 18F-sodium fluoride for oncology using current PET camera technology. J Nucl Med. 2012;53:1175-84. doi:10.2967/jnumed.111.100883.
31. Sgouros G, Roeske JC, McDevitt MR, Palm S, Allen BJ, Fisher DR, et al. MIRD Pamphlet No. 22 (abridged): radiobiology and dosimetry of alpha-particle emitters for targeted radionuclide therapy. J Nucl Med. 2010;51:311-28. doi:10.2967/jnumed.108.058651.
32. Feinendegen LE, McClure JJ. Meeting report - Alpha-emitters for medical therapy - Workshop of the United States Department of Energy - Denver, Colorado, May 30-31, 1996. Radiation Research. 1997;148:195-201. doi:10.2307/3579579.
33. Hatt M, Le Rest CC, Albarghach N, Pradier O, Visvikis D. PET functional volume delineation: a robustness and repeatability study. European Journal of Nuclear Medicine and Molecular Imaging. 2011;38:663-72. doi:10.1007/s00259-010-1688-6.
34. Hatt M, Rest CC-L, Aboagye EO, Kenny LM, Rosso L, Turkheimer FE, et al. Reproducibility of (18)F-FDG and 3 '-Deoxy-3 '-(18)F-Fluorothymidine PET Tumor Volume Measurements. Journal of Nuclear Medicine. 2010;51:1368-76. doi:10.2967/jnumed.110.078501.
35. Kairemo K, Joensuu T. Radium-223-Dichloride in Castration Resistant Metastatic Prostate Cancer-Preliminary Results of the Response Evaluation Using F-18-Fluoride PET/CT. Diagnostics. 2015;5:413-27. doi:10.3390/diagnostics5040413.